ARTICLE

Crustal remelting origin of highly silicic magmatism on the Moon

Bin Su [1], Yi Chen [1,2 ✉], Zongyu Yue[3], Lin Chen [1], Ross N. Mitchell [1,2], Ming Tang[4], Wei Yang [3], Guangyu Huang [1], Jinghui Guo[1], Xian-Hua Li [1] & Fu-Yuan Wu [1]

Orbital observations of non-mare, highly silicic volcanic constructs on the Moon challenge the conventional view of the formation of silicic crusts in the presence of water and plate tectonics—the former the Moon has in very short supply and the latter it likely never ever had. Revealing the silica-rich magma origin may reshape our understanding of early planetary crust formation. However, the cause of lunar silicic magmatism remains enigmatic. Here we conduct phase equilibrium simulations for potential lunar igneous lithologies that demonstrate that the compositions of silicic volcanic constructs can be produced by partial melting of KREEP (potassium, rare earth elements, and phosphorus) basalts. Either internal radiogenic heating or external impact bombardment can provide the heat needed for KREEP basalt melting. Combined with silica-rich materials identified on other rocky planets, we suggest that highly evolved crusts might be more prevalent in the early solar system than anticipated as they can originate from crustal remelting in the absence of water and plate tectonics.

[1] State Key Laboratory of Lithospheric Evolution, Institute of Geology and Geophysics, Chinese Academy of Sciences, Beijing 100029, China. [2] College of Earth and Planetary Sciences, University of Chinese Academy of Sciences, Beijing 100049, China. [3] Key Laboratory of Earth and Planetary Physics, Institute of Geology and Geophysics, Chinese Academy of Sciences, Beijing 100029, China. [4] School of Earth and Space Sciences, Peking University, Beijing 100871, China. ✉email: chenyi@mail.iggcas.ac.cn

Highly silicic magmatism was long thought to be exclusive to Earth. The extensive silicic magmatic rocks on Earth are compositionally diverse and their presence is a mark of crustal maturation[1,2]. In contrast, almost all volcanism on the Moon is basaltic, namely the flood basalts of the maria mostly on the lunar nearside[3,4]. The different magmatic features between the Moon and Earth have usually been ascribed to the absence of water and plate tectonics on the Moon[5,6]. Therefore, it has long been deemed that highly silicic crust or continent-like massifs do not exist on the stagnant-lid Moon.

However, with advances in remote sensing, several non-mare volcanic deposits have been observed on the Moon (Fig. 1), known as spectral "red spots" first recognized in 1972[7]. The spots are characterized by elevated topography with steep slopes (domes, cones, etc.), high albedo, and strong absorption in the ultraviolet relative to the visible region[8–10], with high thorium and low iron contents[11,12]. These features suggest derivation from viscous, evolved magmas with high silica contents, similar to terrestrial rhyolite domes[12]. Their high silica contents are further confirmed by the Diviner Lunar Radiometer Experiment, which shows that these volcanic areas mainly comprise quartz, silica-rich glass, and alkali feldspar[13,14]. High abundances of alkali feldspar and silica with few mafic materials also correspond to the high reflectance of these areas[14,15]. Moreover, a few small granite/felsite clasts (or fragments) were found in returned lunar samples[16,17]. These observations, taken together, provide robust evidence for the presence of highly silicic magmatism on the Moon, thus challenging conventional views of granite petrogenesis on Earth and offering new clues to the Moon's thermal history and crustal evolution.

There are two leading hypotheses for the origin of lunar silicic rocks. The first one, silicate liquid immiscibility (SLI), involves near-complete (90–98%) magma differentiation and then segregation of the residual melt into two immiscible liquids, one being Fe-rich and Si-poor (ferrobasalt), and the other being rich in silica and alkalis (rhyolite)[18,19]. Evidence for SLI on the Moon includes distinct silicate melt inclusions in minerals[18,20] and late-stage mesostasis in mare basalts[21]. This mechanism has been proposed to be responsible for the origin of the small granite clasts/fragments in returned lunar samples[19,22,23]. However, it is unlikely that the microscopic granitic segregations produced by SLI could have formed the massive silicic volcanic constructs (~5–40 km in diameter) such as the Gruithuisen Domes and Hansteen Alpha[12,13,24] (Fig. 1). The silicic volcanic constructs (i.e., large-scale silicic magmatism) have crater-counting ages of ca. 4.0–3.6 billion years ago (Ga)[25–27] that postdate the radiometric ages of returned granite clasts/fragments (4.38–3.88 Ga)[28–30], further suggesting different origins between them. Moreover, high-field-strength elements such as thorium are preferentially partitioned into the Fe-rich, Si-poor liquid instead of the Si-rich liquid (the former having Th content ~2.5 times greater than the latter)[31,32], in apparent contradiction to the high Th contents of lunar red spots[12]. Alternatively, a second hypothesis is crustal remelting[12,13]. This mechanism is widely applied to terrestrial granite petrogenesis[33] and can explain the large volumes and high Th contents of lunar silicic volcanic constructs[34]. However, most lunar samples contain olivine[3], the melting of which only produces limited silica-rich melts. Thus, what kind of lunar lithologies could generate granitic magmas and how remains enigmatic.

To interrogate the feasibility of the crustal remelting mechanism and potentially find out the source rock(s) of the silicic volcanic constructs on the Moon, we conducted phase equilibrium modeling to calculate the partial melting of lunar igneous rocks, including both highland rocks and mare basalts. Thermodynamic models[35] used here are exclusively developed to model the partial melting of basaltic rocks, and thus, mineral assemblages and melt compositions as a function of melting conditions and source rocks can be well constrained[36]. Our work shows that large-scale, highly silicic lunar magmatism can be produced by remelting of KREEP basaltic crust driven by internal radiogenic heating or external impact bombardment.
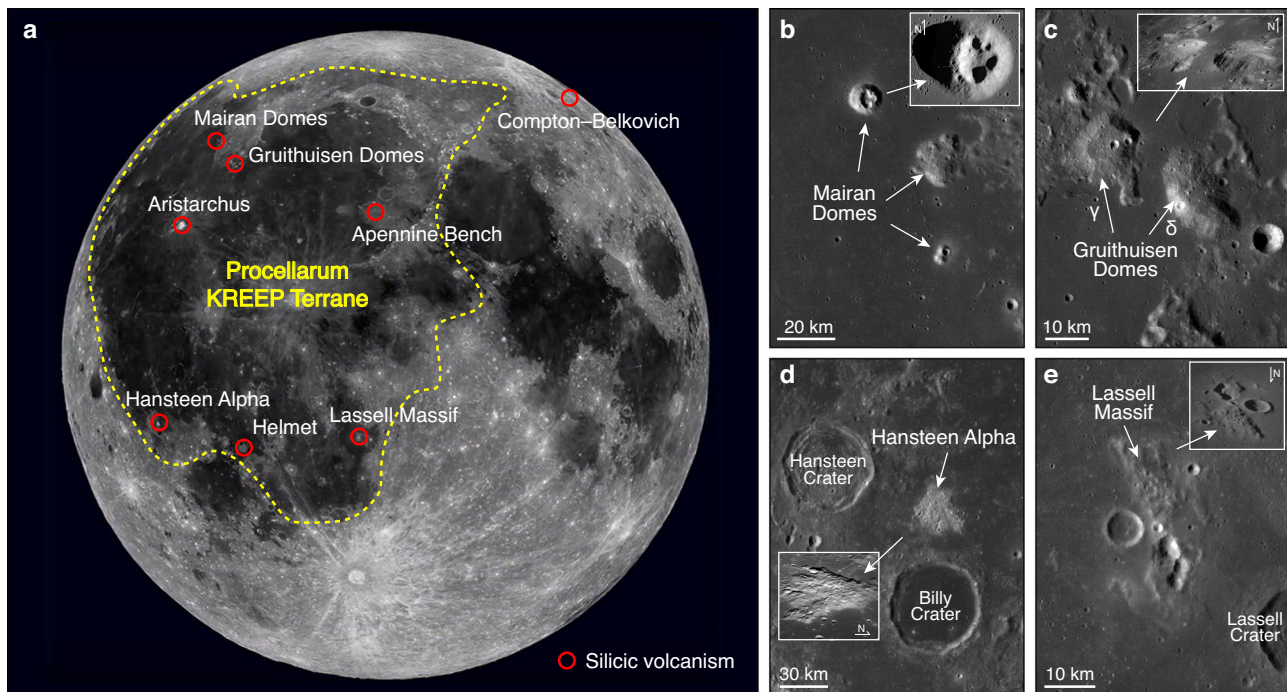
Fig. 1 Silicic volcanic constructs on the Moon. a Locations of silicic volcanic constructs on the Moon (red open circles), with the Procellarum KREEP Terrane outlined (yellow dashed line). The base image is from https://moon.nasa.gov/resources/127/lunar-near-side, published on October 20, 2017. **b–e** Up-close views of the topography of Mairan Domes, Gruithuisen Domes, Hansteen Alpha, and Lassell Massif. Images from the Lunar Reconnaissance Orbiter wide-angle camera and narrow-angle camera (credit: NASA/GSFC/Arizona State University/Lunar QuickMap).

Results

Phase equilibrium modeling of lunar igneous rocks. Lunar igneous rocks modeled here using THERMOCALC v3.47 (see "Methods") include ferroan-anorthositic suite (FANs), Mg-suite, alkali-suite (excluding granite/felsite), KREEP basalts, and low-Ti [$TiO_2 \leq 6$ weight % (wt%)] and high-Ti ($TiO_2 > 6$ wt%) mare basalts. Average bulk-rock compositions[3,37] were used for phase equilibrium modeling (Supplementary Table 1). A series of pressure–temperature phase diagrams were calculated in the range of 800–1500 °C and 0–5 kbar (Fig. 2). Among these rocks, KREEP basalts (together with high-Ti basalts) and Mg-suite rocks have the lowest (840–960 °C) and highest (1130–1180 °C) solidus temperatures, respectively. At subsolidus conditions, lunar igneous rocks all have plagioclase, high-Ca and low-Ca pyroxenes, and ilmenite. K-feldspar is absent in FANs and Mg-suite rocks because of their low bulk K_2O contents. Olivine occurs in most rocks but not in KREEP and high-Ti basalts; instead, they have silica-bearing sub-solidus assemblages, in agreement with petrographic observations (see Supplementary Information for details), indicating that KREEP and high-Ti basalts are more silica-fertile than the other lithologies.

Such fertility can be better understood in the olivine–anorthite–quartz pseudoternary diagram projected from diopside[38] (Fig. 3). Because all stoichiometric plagioclase and pyroxene project along the anorthite–enstatite join, this join defines a thermal divide when plagioclase and pyroxene dominate the residue at low pressures. Bulk compositions on either side of the join have distinct mineral assemblages ranging from quartz-normative to olivine-normative types. Hence, this dividing line can separate lunar rocks into two groups: silica-excess on the right and silica-deficient on the left. KREEP and high-Ti basalts plot on the silica-excess side with the latter much closer to the join, while the other lithologies have average compositions on the silica-deficient side, consistent with our phase equilibrium modeling. Because partial melting paths (or mineral assemblages from subsolidus to liquidus) diverge greatly on opposite sides of the thermal divide[38], silica-excess and silica-deficient lunar rocks are expected to produce different partial melts in terms of silica saturation.

We quantitatively calculated melt compositions for these lunar rocks via phase equilibrium modeling (Supplementary Data 1–6). The contours of melt SiO_2 contents are illustrated in Fig. 2g–l. Partial melts extracted from the silica-deficient FANs, Mg-suite, alkali-suite rocks, and low-Ti basalts are overall basaltic in composition, although a small number of intermediate melts (55–60 wt% SiO_2) can be generated by very low-degree melting of alkali-suite rocks and low-Ti basalts. In contrast, partially melting the silica-excess KREEP and high-Ti basalts produces granitic melts ($SiO_2 > 65$ wt%). Silica contents of the granitic melt along the solidus increase as pressure decreases (Fig. 2j, l). With the temperature increasing, melts from KREEP and high-Ti basalts retain high SiO_2 contents until quartz is exhausted, after which melt compositions become decreasingly silicic over a narrow temperature interval and finally fall into the basaltic range.

Discussion

Highly silicic magmatism from remelting KREEP basalts. Our simulations show that, among all lunar igneous rock types, only KREEP and high-Ti basalts can produce highly silicic melts. However, of the two, high-Ti basalts plot much closer to the thermal divide, and thus, a much narrower parameter space of very low-degree (<5%) melting could yield granitic melts with a high-Ti basalt source (Fig. 4a). Because granitic melts are too viscous to segregate from low melt-fraction (<7%) parental rocks[39], it is unlikely that the large silicic volcanic constructs on the Moon formed from crustal remelting of high-Ti basalts. Also, the volcanic constructs occur mostly far away from high-Ti mare

deposits (Supplementary Fig. 1), further discounting the possibility of a high-Ti basalt origin. Moreover, despite the silica-excess classification of average high-Ti basalts, nearly half of them (~40%) plot on the silica-deficient side of the thermal divide (Fig. 3). Likewise, low-Ti basalts also straddle the thermal divide, of which nearly one-third plot on the silica-excess side but very close to the divide. Hence, neither high-Ti nor low-Ti mare basalts can be considered ideal sources for large-scale, highly silicic magmatism on the Moon.

KREEP basalts, by contrast, have an average composition plotting relatively far from the thermal divide. Moreover, almost all reported KREEP basalts fall to the silica-excess side (Supplementary Fig. 2), in accordance with petrographic observations showing the absence of magnesian olivine and the presence of silica in most KREEP basalts[3]. The non-modal melt compositions calculated along the 1 kbar isobaric melting profile are shown in Fig. 4. For KREEP basalts, granitic melts can be formed by <20% partial melting. With increasing melting degrees, KREEP basalt-derived melts migrate through the andesite field and finally enter the basalt field, while melts from other lunar rocks mainly plot in the basalt field. Furthermore, we also calculated the partial melting of the pristine KREEP (i.e., urKREEP), the last dreg of the magma ocean to solidify, which is proposed to be the parent for KREEP basalts[40,41]. The results show that no granitic melts are present during urKREEP melting beneath the lunar crust (Supplementary Fig. 3). Therefore, KREEP basalts are the best candidate for producing highly silicic magmas on the Moon.

A striking feature of lunar silicic volcanic constructs is high enrichment in Th (up to ~80 $\mu g\,g^{-1}$)[12,42], which can also be achieved by KREEP basalt melting. We combined phase equilibrium and trace-element modeling to compute the Th contents of the silicic melts (see "Methods"). Our modeling shows that KREEP basalt-derived granitic melts have Th contents 2 to 7 times higher than KREEP basalts (Supplementary Table 2). KREEP basalts have average Th contents of 9.3 $\mu g\,g^{-1}$ (ranging from 4.5–14.9 $\mu g\,g^{-1}$)[3]. Thus, the calculated silicic melts have 28–74 $\mu g\,g^{-1}$ Th, matching estimates from remote sensing (~10–80 $\mu g\,g^{-1}$)[12,42]. In contrast, high-Ti and low-Ti mare basalts mostly have Th contents less than 1.5 $\mu g\,g^{-1}$ (ref. [3]), resulting in partial melts only with <15 $\mu g\,g^{-1}$ Th. For major elements, although no lunar missions visited a silicic target, the returned granite clasts/fragments and granitic glasses may provide preliminary constraints on the silicic compositions of the Moon (Supplementary Table 3), with the caveat that these granitic samples are not equivalent to lunar silicic volcanic constructs. Our calculated melt compositions for KREEP basalts are broadly consistent with the present granitic data (Supplementary Fig. 4). Moreover, all but one of the silicic volcanic constructs are confined to the Procellarum KREEP Terrane (PKT), where most KREEP-rich materials were found (Fig. 1). Furthermore, the exception (i.e., Compton–Belkovich volcanic complex) arguably proves the rule in this case as the single occurrence outside the PKT is associated with a rare enrichment of Th on the lunar farside[14]. These arguments collectively support a genetic link between lunar silicic magmatism and KREEP basalts.

Potential formation scenarios. As the silicic volcanic constructs are spatially associated with mare basalts in the PKT, previous work suggested basaltic underplating as a heating mechanism to trigger crustal remelting and produce large volumes of silicic lavas[12,13]. However, mare magmatism in the PKT was active throughout the Nectarian into the Copernican period, mostly from 3.8–3.1 Ga[43–45], enduring much longer than the more ancient and temporally restricted ca. 4.0–3.6 Ga silicic volcanic constructs[25–27]. Moreover, most basaltic plains surrounding the
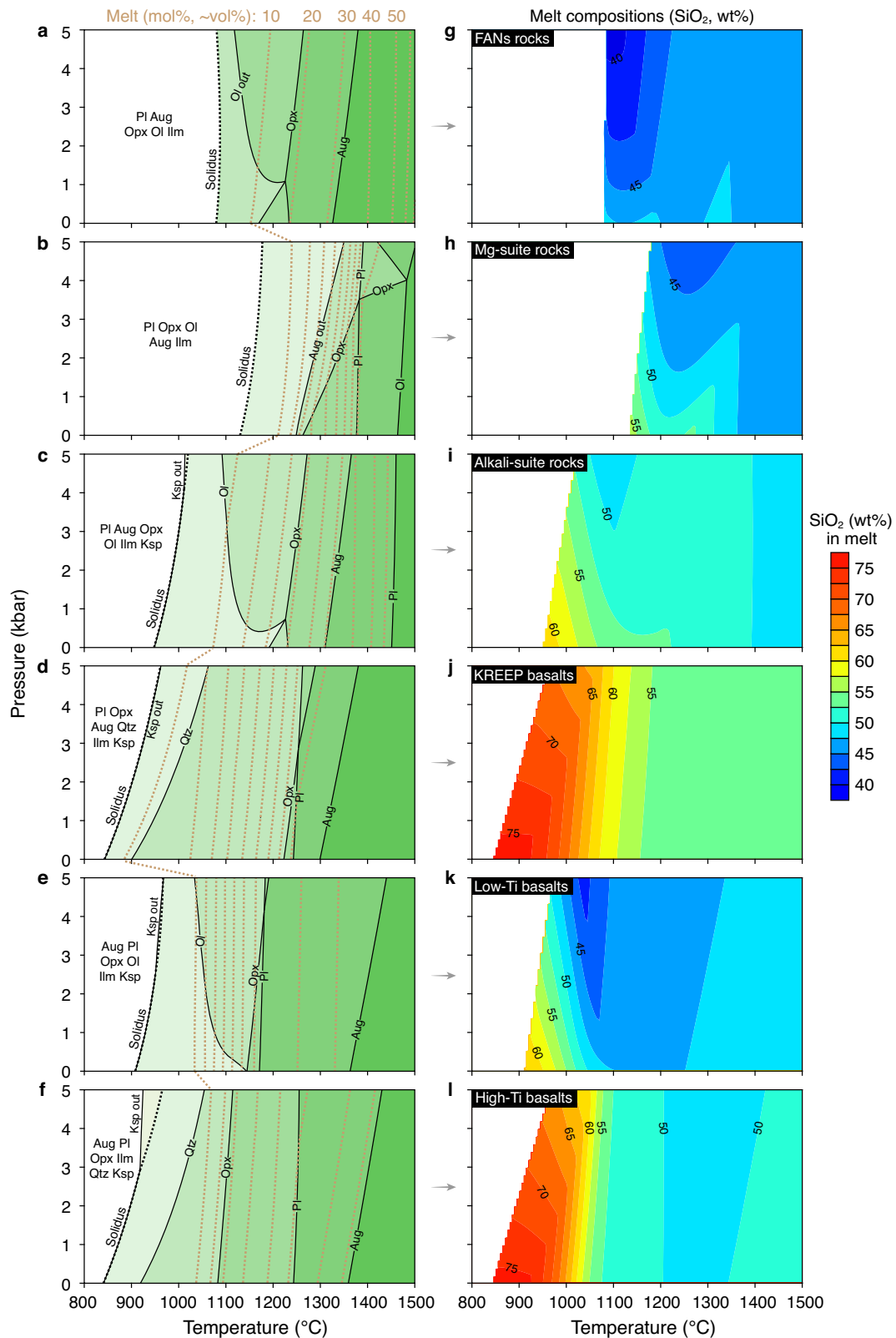
Fig. 2 Phase equilibrium modeling of lunar igneous rocks. a FANs rocks. **b** Mg-suite rocks. **c** Alkali-suite rocks (excluding granite/felsite). **d** KREEP basalts. **e** Low-Ti basalts. **f** High-Ti basalts. Black dashed curves represent the solidi, and brown dashed lines indicate the mole percent (mol%) of partial melts. **g**–**l** Diagrams contoured for melt SiO$_2$ contents. Average bulk compositions of low-Ti and high-Ti basalts are from ref. [37], and the others are from ref. [3] (Supplementary Table 1). Calculated results are shown in Supplementary Data 1–6. Pl plagioclase. Aug augite (high-Ca pyroxene), Opx orthopyroxene (low-Ca pyroxene), Ol olivine, Qtz quartz, Ilm ilmenite, Ksp K-feldspar.
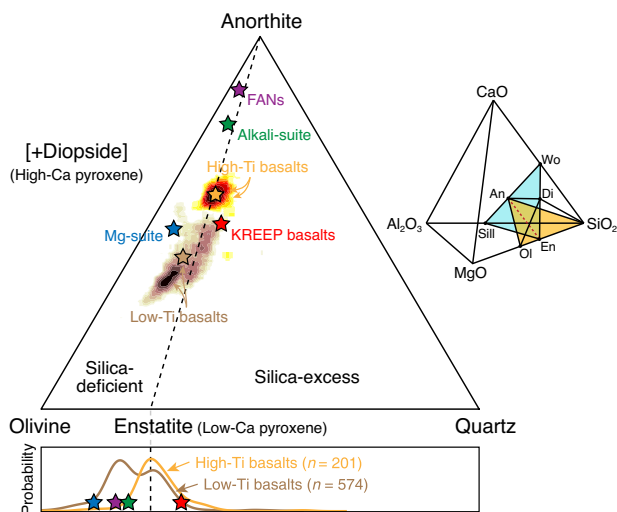
Fig. 3 Lunar igneous rocks in the olivine–anorthite–quartz pseudoternary system projected from diopside. Pentagrams represent average bulk compositions of lunar igneous rocks (FANs rocks, purple; Mg-suite rocks, dark blue; Alkali-suite rocks, green; KREEP basalts, red; Low-Ti basalts, bronze; High-Ti basalts, orange) used in phase equilibrium modeling (Fig. 2). The frequency distributions of high-Ti and low-Ti basalts are shown based on kernel density estimation in the top plot and as probability curves in the bottom plot. The anorthite–enstatite join (dashed line) represents the thermal divide between silica-deficient and silica-excess rocks. Wo wollastonite, En enstatite, Di diopside, An anorthite, Ol olivine, Sill sillimanite.

silicic volcanic constructs are relatively younger[26,42]. These disparate ages complicate the underplating model and must be considered for evaluating if this model is plausible for lunar silicic magma generation.

Alternative mechanisms for KREEP basalt melting include radiogenic heating and meteoritic impact. KREEP basalts have high concentrations of radioactive elements such as K, Th, and U, with an average heat production value of 4.4 ± 1.8 (1σ) μW m^{-3} at 4.0 Ga (calculated after ref. [46]). We used the one-dimensional heat flow equation with terms for radiogenic heat production and conduction to model the thermal evolution (see "Methods"). As a sensitivity test, the models assumed a buried 5-km-thick pile of KREEP basalts within a 40-km-thick crust at variable depths (20–40 km). The initial crustal thermal gradient was fixed to 15 or 20 °C km^{-1} (ref. [47]). The results are illustrated as a series of temperature-time curves with variable levels of heat production (2–7 μW m^{-3}). KREEP basalts near the base of the crust could have been radioactively heated above the solidus for ~100–200 million years after their formation (Fig. 5; Supplementary Fig. 5). This timing is consistent with the relative timing, temporal overlap, and short time interval between KREEP basalt formation (ca. 4.1–3.8 Ga)[43–45] and silicic volcanic construct development (ca. 4.0–3.6 Ga)[25–27]. As burial depths decrease, the role of radiogenic heating would be offset by enhanced thermal diffusion (Fig. 5b, c). Therefore, partial melting of KREEP basalts could have been achieved by internal radiogenic heating preferentially in the deep crust.

As lunar silicic magmatism formed broadly contemporaneously with the ca. 3.9 Ga Late Heavy Bombardment (LHB)[48] and silicic volcanic constructs occur mostly near the edges of impact basins[49], impact melting may be another mechanism for lunar silicic magma formation. To test this scenario, we used the iSALE-2D hydrocode[50,51] to perform two-dimensional impact modeling (see Methods). The models assume a vertical impact of a dunite projectile with a diameter of 20, 40, or 60 km into a
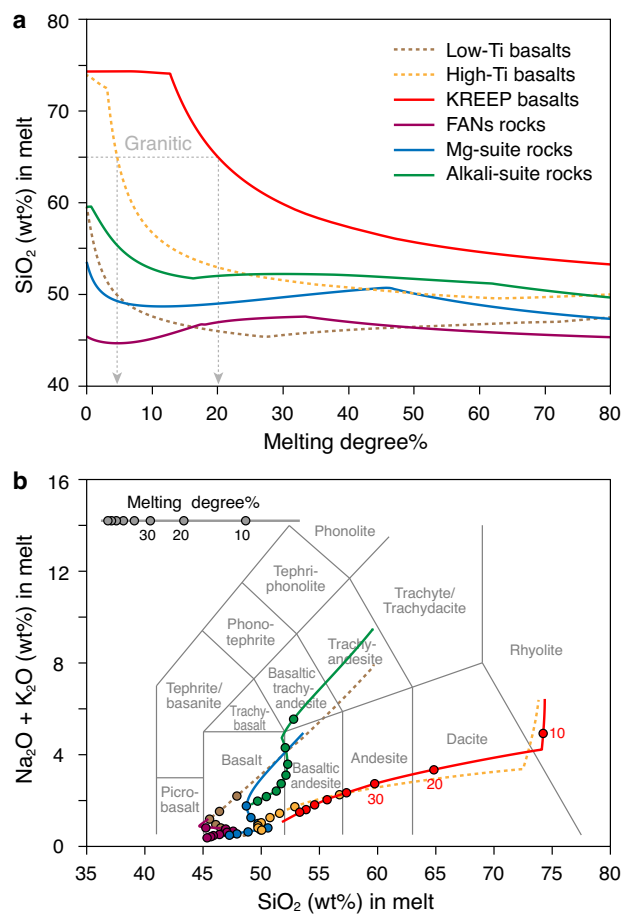

Fig. 4 Modeled melt compositions of lunar igneous rocks. a Melt SiO$_2$ content versus melting degree. Granitic melts (≥65 wt% SiO$_2$; gray dashed lines) can be produced either by very low-degree (<5%) melting of high-Ti basalts or by moderate-degree (<20%) melting of KREEP basalts. b Total alkali-silica diagram showing non-modal batch melt compositions. KREEP basalt-derived melts (red line) plot in the rhyolite–dacite field when melting degrees are <20%. In contrast, partial melts of other lunar rocks (FANs rocks, purple line; Mg-suite rocks, dark blue line; Alkali-suite rocks, green line; Low-Ti basalts, bronze dashed line; High-Ti basalts, orange dashed line) mainly plot in the basalt field. Calculations were conducted at 1 kbar.

40- or 52-km-thick lunar crust[52] with a thermal gradient of 15 or 20 °C km^{-1}, and impact velocity is fixed at 15 km s^{-1} (ref. [53]). The results show that large impacts can produce regional thermal anomalies and form a hot melt pool near the impact site (Fig. 6). At greater distances, the crustal temperature drops gradually, but at shallow depths, there would be a hot layer at temperatures of 850–1000 °C above the solidus of KREEP basalts extending to the edges of impact basins. This model is similar to recent simulations of the early terrestrial bombardment[54] and suggests that impacts could provide the heat needed for KREEP basalt melting in the shallow crust. The silicic volcanism erupting near the Apollo 15 site in the southeast edge of the Mare Imbrium basin, where KREEP basalts are a common component of the region[4], can provide a good example in support of the impact model. Interestingly, the radiogenic and impact melting models make different predictions for melting occurring in the deep or shallow crust, possibly providing a way to discriminate between their relative contributions. Nonetheless, we note that the above models are not mutually exclusive and might be complementary to one another to generate large volumes of silicic magma on the Moon.
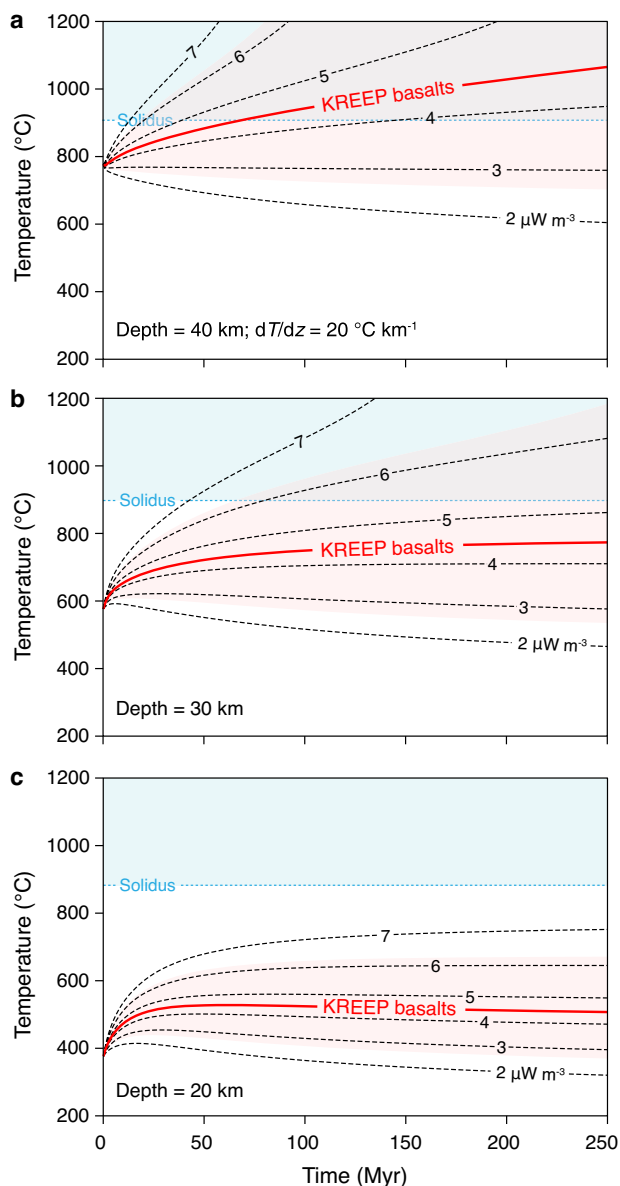
Fig. 5 Radiogenic heating modeling. We assumed burial of a 5-km-thick pile of KREEP basalts within a 40-km-thick crust at depths of 40 km (**a**), 30 km (**b**), or 20 km (**c**), with a thermal gradient (dT/dz) of 20 °C km^{-1} (see Supplementary Fig. 5 for 15 °C km^{-1} results and other conditions). KREEP basalts have 0.54 ± 0.13 (1σ) wt% K$_2$O, 9.3 ± 3.5 µg g^{-1} Th, and 2.6 ± 1.1 µg g^{-1} U (ref. [3]). Their heat production value was 4.4 ± 1.8 µW m^{-3} at 4.0 Ga. The red curves represent the mean values, and the reddish areas cover the full range. The solidus temperatures of KREEP basalts at 40, 30, and 20 km are 911, 896, and 883 °C, respectively.

Implications for silicic magmatism in the solar system. Our modeling demonstrates that remelting KREEP basalts can produce evolved, silica-rich magmas without requiring water and plate tectonics. It was long thought that the siliceous crust is exclusive to Earth. However, evolved, SiO$_2$-rich crustal materials are being increasingly discovered on the Moon[13,14], Venus[55], Mars[56], and some asteroids[57–59], indicating that silicic rocks may constitute a significant part of ancient crusts on rocky bodies in the solar system. Our work indicates that highly silicic magmas can be produced by the partial melting of "silica-excess" (quartz-normative) basaltic rocks under anhydrous conditions in planetary crusts throughout the solar system. The LHB affected the entire inner
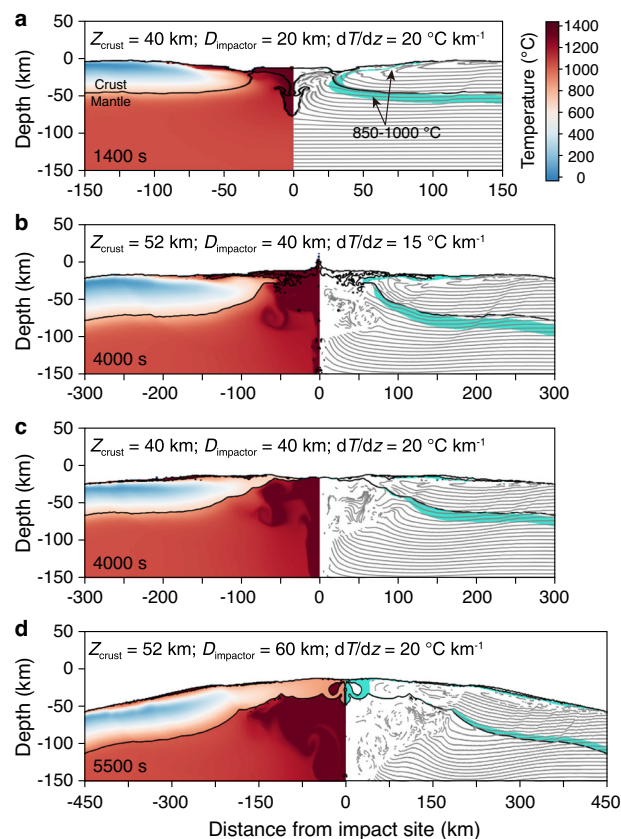
Fig. 6 Hydrocode impact modeling. Post-impact thermal structure for a vertical impact of a dunite impactor with a diameter ($D_{impactor}$) of 20 km (**a**), 40 km (**b, c**), or 60 km (**d**) and an impact velocity of 15 km s^{-1}. The pre-impact crustal thickness (Z_{crust}) was fixed to either 40 km (**a, c**) or 52 km (**b, d**), with a thermal gradient (dT/dz) of 15 °C km^{-1} (**b**) or 20 °C km^{-1} (**a, c, d**). The turquoise areas on the right side show regions of temperatures of 850–1000 °C where partial melting of KREEP basalts could have occurred.

solar system[48] and could have caused melting for early silicic magmatism formation[60]. Such models imply that the early evolved crust on rocky planets might be generated from an older mafic-dominated reservoir. This inference is consistent with our current knowledge of early Earth[54,61,62]. Although Earth's modern felsic crust can be efficiently created in subduction zones[6], the Moon, Mars, Venus, and Mercury seem to lack plate tectonics, and possibly even the early Earth[63]. The silicic magmatism on the stagnant-lid Moon produced by crustal remelting does not require plate tectonics or water and thus provides additional insights into planetary crust formation in the early solar system.

Methods

Phase equilibrium modeling. The modeling was performed using THERMO-CALC version 3.47[64] with the internally consistent thermodynamic dataset ds62 (updated February 2012)[65] in the NCKFMAST (Na$_2$O–CaO–K$_2$O–FeO–MgO–Al$_2$O$_3$–SiO$_2$–TiO$_2$) system. All iron is ferrous, corresponding to the highly reduced conditions of the Moon[66]. The activity–composition solution models used here were as follows: silicate melt, high-Ca pyroxene (augite)[35], low-Ca pyroxene (orthopyroxene), ilmenite[67], plagioclase, K-felspar[68], and olivine[65]. Quartz was treated as a pure phase. These solution models have successfully reproduced the phase relations and partial melting of basaltic rocks[35,36,54]. Thus, they permit quantitative calculations of melt compositions of lunar basaltic igneous rocks (FANs, Mg-suite, alkali-suite rocks, KREEP basalts, and low-Ti and high-Ti mare basalts). Ilmenite saturation is over-predicted under very high-degree melting conditions (other minerals are exhausted) because of the lack of a Ti-bearing endmember in the melt model[35]; nonetheless, it has little influence on our models in terms of low-degree partial melting. Average bulk compositions were employed for phase equilibrium modeling. Bulk compositions of low-Ti and high-Ti mare

basalts are from ref. [37], and the others are from ref. [3] (Supplementary Table 1). All modeling was run under anhydrous conditions due to very low water contents ($\mu g\,g^{-1}$ level) in returned lunar samples[69,70]. Although Bhattacharya et al.[71] conducted spectral and spatial analyses of the silicic Compton–Belkovich volcanic complex and estimated its water content varying from 0.1 to 0.5 wt%, our additional modeling demonstrates that adding water to the dry system of lunar igneous rocks has minimal effect on their melt compositions, especially for SiO_2 contents (Supplementary Fig. 6). Modeled results match well with petrographic observations, verifying the reliability of our simulations. Mineral abundances and melt compositions (non-modal batch melting) calculated in the range of 800–1500 °C and 0–5 kbar are presented in Supplementary Data 1–6.

Trace-element (thorium) modeling. Thorium contents of granitic melts extracted from KREEP basalt melting were calculated using the batch melting equation:

$$C_{melt}/C_{source} = 1/[D + F \times (1 - D)] \qquad (1)$$

where C_{melt} and C_{source} are Th contents of the melt and source rock, respectively, F is the degree of partial melting, and D is the bulk partition coefficient calculated using residual mineral modes and mineral/melt partition coefficients. Mineral and melt modes were obtained by phase equilibrium modeling at 1 bar. The resultant phase proportions are output as mole percent, very close to volume percent. Thus, the weight percent was further calculated using mineral densities from ref. [72]. Most mineral/melt partition coefficients used here were taken from ref. [73], wherein the values are widely used to simulate anatexis of metabasites. Partition coefficients for K-felspar and quartz are from refs. [74,75]. The calculated procedures and results are presented in Supplementary Table 2.

Radiogenic heating modeling. The contribution of radiogenic heating to the melting of KREEP basalt was investigated using the one-dimensional heat flow equation[76]. The standard heat flow equation includes conductive heat flow between rocks of different temperatures, vertical heat transport due to burial or erosion, and heat production by radioactive decay, mechanical deformation, and chemical reaction. Because the vertical heat transport and mechanical and chemical heating can be negligible for lunar crustal rocks, the heat flow equation used here can be simplified as:

$$\frac{\partial T}{\partial t} = \frac{\partial}{\partial z}\left[\kappa(T)\frac{\partial T}{\partial z}\right] + \frac{A_{rad}}{\rho \cdot C_p} \qquad (2)$$

where T is temperature, t is time, κ is thermal diffusivity, z is depth, ρ is density, C_p is specific heat capacity, and A_{rad} is the rate of radiogenic heat production. The models were set with a surface temperature of 250 K, crustal thickness of 40 km, an initial crustal thermal gradient of 15 or 20 °C km^{-1}, a basal temperature of 1300 K at 150 km depth, and a density of KREEP basalt of 3.1 g cm^{-3} (refs. [47,77]). The crust was fixed to comprise a 5-km-thick KREEP basalt layer and a 35-km-thick non-radioactive layer, where the model runs assume variable burial depths of the KREEP basalt layer from 20–40 km. Scenarios shallower than 20 km are not shown because they cannot produce enough heat for KREEP basalt melting. KREEP basalts have 0.54 ± 0.13 (1σ) wt% K_2O, 9.3 ± 3.5 μg g^{-1} Th, and 2.6 ± 1.1 μg g^{-1} U (ref. [3]). Their heat production value was 4.4 ± 1.8 μW m^{-3} at 4.0 Ga, calculated after ref. [46]. As the C_p of different samples is essentially an identical function of temperature[78], the widely used C_p equations provided by ref. [79] were selected here. For the κ, we used the temperature-dependent equation determined on Apollo basalt 10020, 44, because it has relatively low porosity among all measured lunar samples[80]. Also, modeling with variable KREEP basalt thickness (2–7 km) was performed to evaluate its effect on the radiogenic heating mechanism (Supplementary Fig. 5). The results show that the thickness of KREEP basalts should be greater than ~4 km if radiogenic heating alone could raise the temperature above the solidus.

Hydrocode impact modeling. To examine the impact melting process possibly related to the lunar silicic magma formation, we carried out numerical simulations with the shock physics code iSALE-2D[50,51]. The code is based on the SALE (Simplified Arbitrary Lagrangian Eulerian) hydrocode solution algorithm[81] to solve the conservation equations of mass, momentum, and energy. In addition, to describe the thermal and mechanical responses during the hypervelocity impacts, various equations of state and elasto-plastic constitutive models for multiple materials are included[82,83]. More recent improvements include a strength model[50], a porosity compaction model[51,84], and a dilatancy model[50]. The iSALE-2D code has been validated against observations[85] and widely used in simulating lunar basin formation[52,86,87]. In this study, all simulations are axisymmetric, and the projectile vertically impacts a spherical Moon-like target along a central axis. The target has a central gravity field, and it is assumed to have a crust, mantle, and core that are represented by granite, dunite, and iron, respectively. The material models and corresponding parameters derive from ref. [52]. The projectile is represented by dunite because it is a reasonable approximation for typical ordinary chondrite asteroidal material[88–90], and granite is often used as a close analog to the lunar anorthositic crust[89–91]. The pre-impact crustal thickness was fixed to either 40 or 52 km, the surface temperature was 250 K, and the crustal thermal gradient was 15 or 20 °C km^{-1}. To avoid reducing mantle material strength to zero, we

followed refs. [47,52] by imposing an adiabat of 0.04 °C km^{-1} at temperatures above 1,300 K. The mesh resolution was set as a constant with a cell size of 250 × 250 m. The impact velocity was fixed at 15 km s^{-1} (ref. [53]). Because the silicic volcanic constructs occur mostly near the edges of impact basins[49], a dunite impactor with a diameter of 20, 40, or 60 km was employed in our simulations, forming an impact basin ~250, 500, or 800 km in diameter, respectively. Numerical results indicate the above parameter domain is enough to analyze the lunar silicic magma formation. The representative results are presented in Fig. 6, and the corresponding animations are provided in Supplementary Movies 1–4.

Data availability
The data used for phase equilibrium and trace-element modeling and the modeled results are available in the paper, Methods, and Supplementary Materials, and they are also available at https://doi.org/10.6084/m9.figshare.23244101.

Code availability
The software and data files used for phase equilibrium modeling are available at https://hpxeosandthermocalc.org/. The code used for impact modeling is available at https://isale-code.github.io/.

References
1. Dhuime, B., Wuestefeld, A. & Hawkesworth, C. J. Emergence of modern continental crust about 3 billion years ago. *Nat. Geosci.* **8**, 552–555 (2015).
2. Tang, M., Chen, K. & Rudnick, R. L. Archean upper crust transition from mafic to felsic marks the onset of plate tectonics. *Science* **351**, 372–375 (2016).
3. Wieczorek, M. A. et al. The constitution and structure of the lunar interior. *Rev. Mineral. Geochem.* **60**, 221–364 (2006).
4. Shearer, C. K. et al. Thermal and magmatic evolution of the moon. *Rev. Mineral. Geochem.* **60**, 365–518 (2006).
5. Campbell, I. H. & Taylor, S. R. No water, no granites-No oceans, no continents. *Geophys. Res. Lett.* **10**, 1061–1064 (1983).
6. Arndt, N. T. The formation and evolution of the continental crust. *Geochem. Perspect.* **2**, 405–533 (2013).
7. Whitaker, E. A. Lunar color boundaries and their relationship to topographic features: a preliminary survey. *The Moon* **4**, 348–355 (1972).
8. Head, J. W. & McCord, T. B. Imbrian-age highland volcanism on the moon: the Gruithuisen and Mairan domes. *Science* **199**, 1433–1436 (1978).
9. Hawke, B. R. et al. Hansteen alpha: a volcanic construct in the lunar highlands. *J. Geophys. Res. Planets* **108**, 5069 (2003).
10. Greenhagen, B. T. et al. Global silicate mineralogy of the Moon from the Diviner Lunar Radiometer. *Science* **329**, 1507–1509 (2010).
11. Lucey, P. G., Blewett, D. T. & Jolliff, B. L. Lunar iron and titanium abundance algorithms based on final processing of Clementine ultraviolet-visible images. *J. Geophys. Res. Planets* **105**, 20297–20305 (2000).
12. Hagerty, J. J. et al. Refined thorium abundances for lunar red spots: implications for evolved, nonmare volcanism on the Moon. *J. Geophys. Res. Planets* **111**, E06002 (2006).
13. Glotch, T. D. et al. Highly silicic compositions on the Moon. *Science* **329**, 1510–1513 (2010).
14. Jolliff, B. L. et al. Non-mare silicic volcanism on the lunar farside at Compton–Belkovich. *Nat. Geosci.* **4**, 566–571 (2011).
15. Clegg-Watkins, R. et al. Nonmare volcanism on the Moon: photometric evidence for the presence of evolved silicic materials. *Icarus* **285**, 169–184 (2017).
16. Warren, P. H. et al. Petrology and chemistry of two "large" granite clasts from the Moon. *Earth Planet. Sci. Lett.* **64**, 175–185 (1983).
17. Seddio, S. M., Jolliff, B. L., Korotev, R. L. & Zeigler, R. A. Petrology and geochemistry of lunar granite 12032,366-19 and implications for lunar granite petrogenesis. *Am. Mineral.* **98**, 1697–1713 (2013).
18. Roedder, E. & Weiblen, P. W. Lunar petrology of silicate melt inclusions, Apollo 11 rocks. *Proc. Apollo 11 Lunar Sci. Confer.* **1**, 801–837 (1970).
19. Rutherford, M. J., Hess, P. C. & Daniel, G. H. Experimental liquid line of descent and liquid immiscibility for basalt 70017. *Proc. Lunar Planet. Sci. Confer.* **5**, 569–583 (1974).
20. Roedder, E. & Weiblen, P. W. Petrology of silicate melt inclusions, Apollo 11 and Apollo 12 and terrestrial equivalents. *Proc. Lunar Planet. Sci. Confer.* **2**, 507–528 (1971).

21. Warner, R. D., Taylor, G. J., Mansker, W. L. & Keil, K. Clast assemblages of possible deep-seated/77517/and immiscible-melt/77538/origins in Apollo 17 breccias. *Proc. Lunar Planet. Sci. Confer.* **9**, 941–958 (1978).

22. Jolliff, B., Floss, C., McCallum, I. & Schwartz, J. Geochemistry, petrology, and cooling history of 14161, 7373: A plutonic lunar sample with textural evidence of granitic-fraction separation by silicate-liquid immiscibility. *Am. Mineral.* **84**, 821–837 (1999).

23. Yang, J. et al. Significance of silicate liquid immiscibility for the origin of young highly evolved lithic clasts in Chang'E-5 regolith. *Geochim. Cosmochim. Acta* **340**, 189–205 (2023).

24. Taylor, G. et al. Silicate liquid immiscibility, evolved lunar rocks and the formation of KREEP, In *Proc Conference on the Lunar Highlands Crust* (eds. Papike, J. J. & Merrill, R. B) 339–352 (1980).

25. Wagner, R., Head Iii, J. W., Wolf, U. & Neukum, G. Stratigraphic sequence and ages of volcanic units in the Gruithuisen region of the Moon. *J. Geophys. Res. Planets* **107**, 5104 (2002).

26. Wagner, R., Head, J. W. III, Wolf, U. & Neukum, G. Lunar red spots: Stratigraphic sequence and ages of domes and plains in the Hansteen and Helmet regions on the lunar nearside. *J. Geophys. Res. Planets* **115**, E06015 (2010).

27. Ashley, J. W. et al. The Lassell massif—a silicic lunar volcano. *Icarus* **273**, 248–261 (2016).

28. Meyer, C., Williams, I. S. & Compston, W. Uranium-lead ages for lunar zircons: evidence for a prolonged period of granophyre formation from 4.32 to 3.88 Ga. *Meteorit. Planet. Sci.* **31**, 370–387 (1996).

29. Zhang, A.-C. et al. Thermal history of Apollo 12 granite and KREEP-rich rock: Clues from Pb/Pb ages of zircon in lunar breccia 12013. *Geochim. Cosmochim. Acta* **95**, 1–14 (2012).

30. Zeng, X. et al. Oldest immiscible silica-rich melt on the Moon recorded in a ~4.38 Ga zircon. *Geophys. Res. Lett.* **47**, e2019GL085997 (2020).

31. Neal, C. R. & Taylor, L. A. The nature and barium partitioning between immiscible melts: a comparison of experimental and natural systems with reference to lunar granite petrogenesis. *Proc. Lunar Planet. Sci. Confer.* **19**, 209–218 (1989).

32. Shearer, C. K., Papike, J. J. & Spilde, M. N. Trace-element partitioning between immiscible lunar melts: an example from naturally occurring lunar melt inclusions. *Am. Mineral.* **86**, 238–246 (2001).

33. Bergantz, G. W. Underplating and partial melting: implications for melt generation and extraction. *Science* **245**, 1093–1095 (1989).

34. Gullikson, A. L. et al. Silicic lunar volcanism: Testing the crustal melting model. *Am. Mineral.* **101**, 2312–2321 (2016).

35. Green, E. et al. Activity–composition relations for the calculation of partial melting equilibria in metabasic rocks. *J. Metamorph. Geol.* **34**, 845–869 (2016).

36. Palin, R. M. et al. High-grade metamorphism and partial melting of basic and intermediate rocks. *J. Metamorph. Geol.* **34**, 871–892 (2016).

37. Cone, K. A. ApolloBasalt DB_V2, Version 1.0. *Interdisciplinary earth data alliance (IEDA).* https://doi.org/10.26022/IEDA/111982 (2021).

38. O'Hara, M. The bearing of phase equilibria studies in synthetic and natural systems on the origin and evolution of basic and ultrabasic rocks. *Earth Sci. Rev.* **4**, 69–133 (1968).

39. Rosenberg, C. L. & Handy, M. R. Experimental deformation of partially melted granite revisited: implications for the continental crust. *J. Metamorph. Geol.* **23**, 19–28 (2005).

40. Warren, P. H. & Wasson, J. T. The origin of KREEP. *Rev. Geophys.* **17**, 73–88 (1979).

41. Neal, C. & Taylor, L. Definition of pristing, unadulterated urKREEP composition using the "K-FRAC/REEP-FRAC" hypothesis. *Proc. Lunar Planet. Sci. Confer.* **20**, 772–773 (1989).

42. Glotch, T. D. et al. The Mairan domes: Silicic volcanic constructs on the Moon. *Geophys. Res. Lett.* **38**, L21204 (2011).

43. Nyquist, L. E. & Shih, C. Y. The isotopic record of lunar volcanism. *Geochim. Cosmochim. Acta* **56**, 2213–2234 (1992).

44. Mitchell, R. N. Chang'E-5 reveals the Moon's secrets to a longer life. *Innovation* **2**, 100177 (2021).

45. Shih, C. Y., Nyquist, L. E., Bansal, B. & Wiesmann, H. Rb-Sr and Sm-Nd chronology of an Apollo 17 KREEP basalt. *Earth Planet. Sci. Lett.* **108**, 203–215 (1992).

46. Kramers, J. D., Kreissig, K. & Jones, M. Q. W. Crustal heat production and style of metamorphism: a comparison between two Archean high grade provinces in the Limpopo Belt, southern Africa. *Precambr. Res.* **112**, 149–163 (2001).

47. Melosh, H. et al. The origin of lunar mascon basins. *Science* **340**, 1552–1555 (2013).

48. Strom, R. G. et al. The origin of planetary impactors in the inner solar system. *Science* **309**, 1847–1850 (2005).

49. Chauhan, M. Silicic volcanism on the Moon. In *Encyclopedia of Lunar Science* (eds. Cudnik, B.) (Springer, Cham, 2018).

50. Collins, G. S., Melosh, H. J. & Ivanov, B. A. Modeling damage and deformation in impact simulations. *Meteorit. Planet. Sci.* **39**, 217–231 (2004).

51. Wünnemann, K., Collins, G. S. & Melosh, H. J. A strain-based porosity model for use in hydrocode simulations of impacts and implications for transient crater growth in porous targets. *Icarus* **180**, 514–527 (2006).

52. Johnson, B. C. et al. Formation of the Orientale lunar multiring basin. *Science* **354**, 441–444 (2016).

53. Le Feuvre, M. & Wieczorek, M. A. Nonuniform cratering of the Moon and a revised crater chronology of the inner Solar System. *Icarus* **214**, 1–20 (2011).

54. Johnson, T. E. et al. An impact melt origin for Earth's oldest known evolved rocks. *Nat. Geosci.* **11**, 795–799 (2018).

55. Gilmore, M., Treiman, A., Helbert, J. & Smrekar, S. Venus surface composition constrained by observation and experiment. *Space Sci. Rev.* **212**, 1511–1540 (2017).

56. Christensen, P. et al. Evidence for magmatic evolution and diversity on Mars from infrared observations. *Nature* **436**, 504–509 (2005).

57. Day, J. M. D. et al. Early formation of evolved asteroidal crust. *Nature* **457**, 179–182 (2009).

58. Hahn, T. M. Jr. et al. Dacite formation on Vesta: partial melting of the eucritic crust. *Meteorit. Planet. Sci.* **52**, 1173–1196 (2017).

59. Nicklas, R. W., Day, J., Gardner-Vandy, K. G. & Udry, A. Early silicic magmatism on a differentiated asteroid. *Nat. Geosci.* **15**, 696–699 (2022).

60. Johnson, T. E. et al. Giant impacts and the origin and evolution of continents. *Nature* **608**, 330–335 (2022).

61. O'Neil, J., Carlson, R. W., Francis, D. & Stevenson, R. K. Neodymium-142 evidence for Hadean mafic crust. *Science* **321**, 1828–1831 (2008).

62. Reimink, J. et al. No evidence for Hadean continental crust within Earth's oldest evolved rock unit. *Nat. Geosci.* **9**, 777–780 (2016).

63. Palin, R. M. et al. Secular change and the onset of plate tectonics on Earth. *Earth Sci. Rev.* **207**, 103172 (2020).

64. Powell, R. & Holland, T. J. B. An internally consistent dataset with uncertainties and correlations: 3. Applications to geobarometry, worked examples and a computer-program. *J. Metamorph. Geol.* **6**, 173–204 (1988).

65. Holland, T. J. B. & Powell, R. An improved and extended internally consistent thermodynamic dataset for phases of petrological interest, involving a new equation of state for solids. *J. Metamorph. Geol.* **29**, 333–383 (2011).

66. Wadhwa, M. Redox conditions on small bodies, the Moon and Mars. *Rev. Mineral. Geochem.* **68**, 493–510 (2008).

67. White, R. W. et al. New mineral activity–composition relations for thermodynamic calculations in metapelitic systems. *J. Metamorph. Geol.* **32**, 261–286 (2014).

68. Holland, T. J. B. & Powell, R. Activity–composition relations for phases in petrological calculations: an asymmetric multicomponent formulation. *Contrib. Mineral. Petrol.* **145**, 492–501 (2003).

69. Saal, A. E. et al. Volatile content of lunar volcanic glasses and the presence of water in the Moon's interior. *Nature* **454**, 192–195 (2008).

70. Hui, H., Peslier, A. H., Zhang, Y. & Neal, C. R. Water in lunar anorthosites and evidence for a wet early Moon. *Nat. Geosci.* **6**, 177–180 (2013).

71. Bhattacharya, S. et al. Endogenic water on the Moon associated with non-mare silicic volcanism: implications for hydrated lunar interior. *Curr. Sci.* **105**, 685–691 (2013).

72. Srinivasan, P. et al. Silica-rich volcanism in the early solar system dated at 4.565 Ga. *Nat. Commun.* **9**, 3036 (2018).

73. Bédard, J. H. A catalytic delamination-driven model for coupled genesis of Archaean crust and sub-continental lithospheric mantle. *Geochim. Cosmochim. Acta* **70**, 1188–1214 (2006).

74. Nash, W. P. & Crecraft, H. R. Partition-coefficients for trace-elements in silicic magmas. *Geochim. Cosmochim. Acta* **49**, 2309–2322 (1985).

75. Bea, F., Pereira, M. D. & Stroh, A. Mineral/leucosome trace-element partitioning in a peraluminous migmatite (a laser ablation–ICP-MS study). *Chem. Geol.* **117**, 291–312 (1994).

76. Clark, C., Fitzsimons, I. C. W., Healy, D. & Harley, S. L. How does the continental crust get really hot? *Elements* **7**, 235–240 (2011).

77. Wieczorek, M. A. & Phillips, R. J. The "Procellarum KREEP Terrane": implications for mare volcanism and lunar evolution. *J. Geophys. Res. Planets* **105**, 20417–20430 (2000).

78. Horai, K. & Fujii, N. Thermophysical properties of lunar material returned by Apollo missions. *Moon* **4**, 447–475 (1972).

79. Whittington, A. G., Hofmeister, A. M. & Nabelek, P. I. Temperature-dependent thermal diffusivity of the Earth's crust and implications for magmatism. *Nature* **458**, 319–321 (2009).

80. Horai, K. & Winkler, J. L. Jr Thermal diffusivity of two Apollo 11 samples, 10020,44 and 10065,23: Effect of petrofabrics on the thermal conductivity of porous lunar rocks under vacuum. *Proc. Lunar Planet. Sci. Confer.* **11**, 1777–1788 (1980).

81. Amsden, A., Ruppel, H. & Hirt, C. *SALE: a Simplified ALE Computer Program for Fluid Flow at All Speeds* (US Department of Commerce, National Technical Information Service, 1980).

82. Melosh, H. J., Ryan, E. V. & Asphaug, E. Dynamic fragmentation in impacts-hydrocode simulation of laboratory impacts. *J. Geophys. Res. Planets* **97**, 14735–14759 (1992).

83. Ivanov, B. A., Deniem, D. & Neukum, G. Implementation of dynamic strength models into 2D hydrocodes: Applications for atmospheric breakup and impact cratering. *Int. J. Impact Eng.* **20**, 411–430 (1997).

84. Collins, G., Melosh, H. & Wünnemann, K. Improvements to the ε-α porous compaction model for simulating impacts into high-porosity solar system objects. *Int. J. Impact Eng.* **38**, 434–439 (2011).

85. Pierazzo, E. et al. Validation of numerical codes for impact and explosion cratering: Impacts on strengthless and metal targets. *Meteorit. Planet. Sci.* **43**, 1917–1938 (2008).

86. Potter, R. W. et al. Constraining the size of the South Pole-Aitken basin impact. *Icarus* **220**, 730–743 (2012).

87. Potter, R. W. et al. Numerical modeling of the formation and structure of the Orientale impact basin. *J. Geophys. Res. Planets* **118**, 963–979 (2013).

88. Pierazzo, E., Kring, D. A. & Melosh, H. J. Hydrocode simulation of the Chicxulub impact event and the production of climatically active gases. *J. Geophys. Res. Planets* **103**, 28607–28625 (1998).

89. Yue, Z. et al. Projectile remnants in central peaks of lunar impact craters. *Nat. Geosci.* **6**, 435–437 (2013).

90. Silber, E. A., Osinski, G. R., Johnson, B. C. & Grieve, R. A. Effect of impact velocity and acoustic fluidization on the simple-to-complex transition of lunar craters. *J. Geophys. Res. Planets* **122**, 800–821 (2017).

91. Collins, G. Numerical simulations of impact crater formation with dilatancy. *J. Geophys. Res. Planets* **119**, 2600–2619 (2014).

Author contributions
Y.C. led the study. B.S. conducted the phase equilibrium and trace-element modeling. Z.Y. conducted the hydrocode impact modeling. L.C. conducted the radiogenic heating modeling. R.N.M., M.T., W.Y., G.H., J.G., X.-H.L., and F.-Y.W. contributed to the interpretation of the results. B.S. and Y.C. wrote the manuscript with input from all authors.

Competing interests
The authors declare no competing interests.

Additional information
Supplementary information The online version contains supplementary material available at https://doi.org/10.1038/s43247-023-00900-8.

Correspondence and requests for materials should be addressed to Yi Chen.

Peer review information *Communications Earth & Environment* thanks Timmons Erickson and the other, anonymous, reviewer(s) for their contribution to the peer review of this work. Primary Handling Editor: Joe Aslin. A peer review file is available

Reprints and permission information is available at http://www.nature.com/reprints

Publisher's note Springer Nature remains neutral with regard to jurisdictional claims in published maps and institutional affiliations.